THE JOURNAL OF PHYSICAL CHEMISTRY A
A JOURNAL OF THE AMERICAN CHEMICAL SOCIETY

pubs.acs.org/JPCA Article

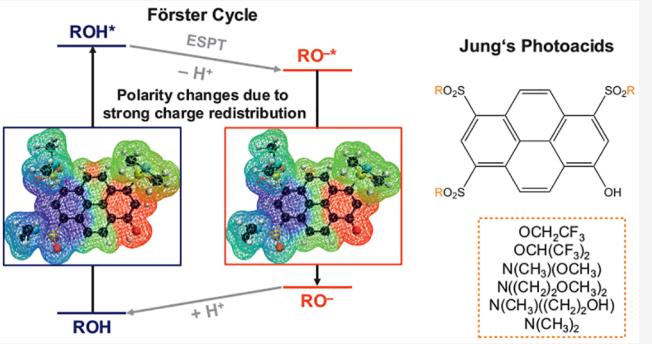
Theoretical Study on the Photoacidity of Hydroxypyrene Derivatives in DMSO Using ADC(2) and CC2

Niklas Sülzner* and Christof Hättig

Cite This: https://doi.org/10.1021/acs.jpca.2c04436 Read Online

ACCESS | Metrics & More | Article Recommendations | Supporting Information

ABSTRACT: This work applies the thermodynamic Förster cycle to theoretically investigate the pK_a^*, i.e., excited-state pK_a values of pyranine-derived superphotoacids developed by Jung and co-workers. The latter photoacids are strong enough to transfer a proton to the aprotic solvent dimethyl sulfoxide (DMSO). The Förster cycle provides access to pK_a^* via the ground-state pK_a and the electronic excitation energies. We use the conductor-like screening model for real solvents (COSMO-RS) to compute the ground-state pK_a and the correlated wavefunction-based methods ADC(2) and CC2 with the continuum solvation model COSMO to calculate the pK_a change upon excitation. A comparison of the calculated UV/Vis absorption and fluorescence emission energies to the experimental results leads us to infer that this approach allows for a proper description of the electronic excitations. In particular, implicit solvation by means of the COSMO model appears to be sufficient for the treatment of these photoacids in DMSO. The calculations confirm the presumption that a charge redistribution from the hydroxy group to the aromatic ring and the electron-withdrawing substituents is the origin of photoacidity for these photoacids. Moreover, the calculations with the continuum solvation model predict that the pK_a jump upon excitation decreases with increasing solvent polarity, as rationalized based on the Förster cycle.



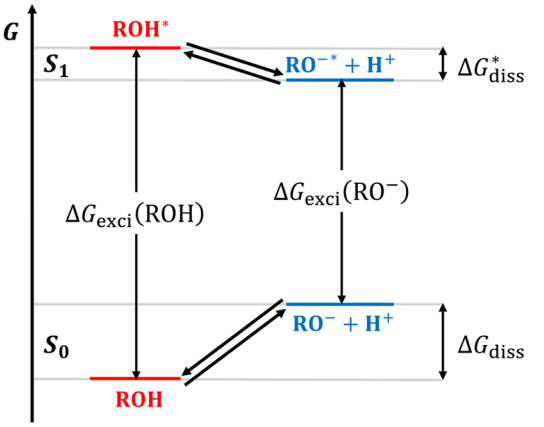
Downloaded via BOCHUM LIBRARIES on August 30, 2022 at 08:18:34 (UTC).
See https://pubs.acs.org/sharingguidelines for options on how to legitimately share published articles.

INTRODUCTION

Proton transfer belongs to the most important elementary reactions taking part in various chemical, biochemical, and biological processes.[1−3] To elucidate the precise mechanisms of proton-transfer reactions, i.e., possible intermediates such as contact ion pairs and rate constants of the individual steps, so-called photoacids have proven particularly powerful tools.[4−22] These photoacids are molecules that exhibit an acidity increase, i.e., a decrease in pK_a, upon electronic excitation, which can trigger an excited-state proton transfer (ESPT) to a suitable proton acceptor.[23,24] Due to limited acid strengths, the use of most photoacids was restricted to the study of ESPT in water[4] or aqueous solutions containing either an additional base[5] or a cosolvent.[6−9] Only special photoacids, referred to as superphotoacids, are particularly strong and exhibit in water negative pK_a values in the excited state,[25−28] which often also allows them to perform an ESPT in neat protic[10−12] or even aprotic solvents.[13−22]

Originally, it was Förster who pointed out that photoacidity can be explained by a thermodynamic cycle that includes the proton-transfer equilibria for the electronic ground and the excited state.[29,30] Based on this so-called Förster cycle (Scheme 1), the excited-state pK_a value, from now on denoted pK_a^*, can be obtained from the ground-state pK_a value and the Gibbs free energy differences between the ground and the excited state of the acid (ROH) and its conjugate base (RO^-):

Scheme 1. Förster Cycle



Received: June 27, 2022
Revised: August 3, 2022

© XXXX The Authors. Published by American Chemical Society

$$pK_a^* = pK_a + \frac{\Delta G_{exci}(RO^-) - \Delta G_{exci}(ROH)}{RT \ln(10)} \quad (1)$$

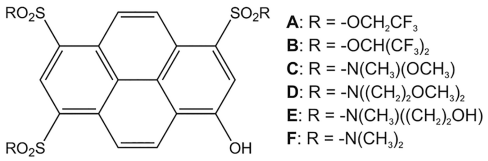
with the excitation Gibbs free energies $\Delta G_{exci}(ROH)$ and $\Delta G_{exci}(RO^-)$ of the two species, the ideal gas constant R, and the absolute temperature T. If used to calculate pK_a^*, the accuracy of the results thus depends on the accuracy of these input quantities. Nevertheless, it is the standard approach to determine pK_a^* in experimental as well as in theoretical investigations since it is usually not possible to measure pK_a^* as an equilibrium quantity.

Measurements of pK_a values are in particular difficult in nonaqueous, aprotic solution.[31−33] For these solvents, theoretical pK_a prediction tools are crucial.[34,35] Different methods are nowadays available,[36,37] including the conductor-like screening model for real solvents (COSMO-RS).[38−42] COSMO-RS is an extension of the conductor-like screening model (COSMO)[43,44] to reintroduce specific solute−solvent interactions and it has been already successfully applied to pK_a calculations in water,[45,46] dimethyl sulfoxide (DMSO),[45] acetonitrile,[47] and acetone.[48]

Until today, only few examples of theoretical pK_a^* predictions are reported in the literature, using quantum chemical calculations[49−56] as well as molecular dynamics (MD) simulations with hybrid quantum-mechanics/molecular-mechanics (QM/MM) techniques.[57−60] Some theoretical studies on photoacids also attempt to directly address the ESPT process by modeling its reaction mechanism or providing information on the molecular factors governing photoacidity, e.g., the electronic structure.[61−69] Recently, also the first *ab initio* (QM/MM) MD simulations on the excited-state dynamics of photoacids were reported, e.g., on the vibrational dynamics of 8-hydroxypyrene-1,3,6-trisulfonate (HTPS or pyranine) in neat water[70,71] or acetate-containing aqueous solution,[72,73] the ESPT dynamics of HPTS in 1-methylimidazole[74] or water,[75] and the ESPT dynamics of the superphotoacid quinone cyanine 9 (QCy9) in water.[76] However, all of these have in common that they are typically limited to time-dependent density functional theory (TDDFT) for the description of electronic excitations, which gives sometimes wrong shapes for the excited state potential energy curves.[77] Apart from the known deficiency of TDDFT regarding charge-transfer excitations, which could be avoided by using long-range-adapted functionals such as CAM-B3-LYP, the rather low accuracy in excitation energies still remains a problem. In the extreme, this can lead to qualitatively wrong results, e.g., a different order of the excited states as recently reported by Acharya et al. for the photoacid naphthol.[78] To the best of our knowledge, no comparable approach to the full pK_a^* beyond TDDFT that uses accurate correlated wavefunction-based methods (e.g., the algebraic diagrammatic construction scheme through second order ADC(2) or the approximate coupled cluster singles and doubles method CC2) instead has yet been reported.

In this study, we focus on the non-charged HPTS derivatives introduced by Jung and co-workers (Scheme 2).[14] These are obtained by functionalizing the sulfonate groups with electron-withdrawing ester (**A**−**B**) and amide (**D**−**F**) moieties. The solvatochromic properties[15] as well as ESPT kinetics[14,16] have been studied experimentally in a variety of solvents including water, methanol, ethanol, and DMSO. Recently, the dynamics and ESPT intermediates of a strongly hydrogen-bonded complex of compound **A** with a trialkylphosphine oxide in nitrile solution were elucidated.[79,80] Furthermore, for the strongest superphotoacid **B** of that class, namely tris-(1,1,1,3,3,3-hexafluoropropan-2-yl)-8-hydroxypyrene-1,3,6-trisulfonate ($pK_a^* \approx -4$ in water),[14] the possibility of ESPT in acetone−water mixtures[81] and in neat acetone were demonstrated.[82] Despite the wealth of experimental knowledge regarding this photoacid, only limited information on the molecular origin of the exceptionally high photoacidity is yet available in the literature.

Scheme 2. Molecular Structures of Jung's Photoacids A−F with the Different Substituents R



Here we apply the Förster cycle to theoretically predict the pK_a^* values of these pyranine-derived photoacids in the polar, aprotic solvent DMSO, which we choose because of the amount of experimental spectroscopic reference data for this class of photoacids in this solvent. Moreover, from a computational point of view, this solvent is a good compromise in accuracy for the implicit solvent model COSMO as it is both aprotic and polar. As a dielectric continuum solvation model, COSMO is restricted to purely electrostatic solute−solvent interactions and poorly describes specific interactions, e.g., hydrogen bonding. This approach provides access to pK_a^* via the ground-state pK_a and the electronic excitation energies. To the best of our knowledge, this is the first attempt that uses highly accurate wavefunction-based methods for pK_a^* prediction.

First, a brief comparison of calculations at different levels of theory for the geometries and excitation energies is used to establish our defaults for computing electronic UV/Vis absorption and emission spectra. These tools are then used to thoroughly review the results for one selected photoacid with the methods ADC(2) and CC2 with and without COSMO to disentangle individual effects on the electronic excitation energies. Next, we compare the calculated UV/Vis absorption and fluorescence emission energies in DMSO with experimental spectra to quantify the accuracy of the results. Here, the focus will be on the differences between absorption and emission spectra, and between the protonated and deprotonated species. Finally, we compute pK_a^* values of the photoacids in DMSO using the calculated results and analyze the individual contributions to and the solvent effect on this quantity.

METHODS

All electronic structure calculations were done with the TURBOMOLE program package (version 7.4).[83,84] Second order Møller−Plesset perturbation theory (MP2), ADC(2), and CC2 calculations (with the ricc2 program) routinely used the resolution-of-the-identity (RI) approximation for the electron repulsion integrals and the frozen-core approximation for the 1s orbitals at C, N, O, F and the 1s2s2p orbitals at S. The integral screening threshold for the MO calculations ($scftol) was lowered to 10^{-15} to ensure convergence with diffuse basis functions. Solution-phase calculations refer to the solvent DMSO as described by the COSMO model with $\epsilon_r = 46.45$ for the (relative) dielectric constant and $n = 1.479$ for the refractive index. Default cavity parameters were used unless stated differently. For the calculation of electronic excitation

https://doi.org/10.1021/acs.jpca.2c04436
J. Phys. Chem. A XXXX, XXX, XXX−XXX

Table 1. Comparison of Vertical Electronic Excitation Energies in eV for the First Transition with Different Combinations of Equilibrium Structures for S_0 or S_1 (Rows) and Methods for the Calculation of the Electronic Excitation Energy (Columns) of the Protonated and Deprotonated Species of Photoacid F

		excitation energies			
	geometries	ADC(2)	COSMO-ADC(2)	CC2	COSMO-CC2
			acid		
S_0	MP2	3.108	2.975	3.168	3.016
	COSMO-MP2	3.096	2.957	3.156	2.999
	CC2	3.067	2.929	3.130	2.975
	COSMO-CC2	3.055	2.910	3.120	2.958
S_1	ADC(2)	2.765	2.602	2.862	2.690
	COSMO-ADC(2)	2.733	2.547	2.844	2.655
	CC2	2.759	2.599	2.852	2.683
			base		
S_0	MP2	2.171	2.134	2.350	2.251
	COSMO-MP2	2.160	2.174	2.350	2.283
	CC2	2.143	2.107	2.329	2.229
	COSMO-CC2	2.135	2.135	2.332	2.253
S_1	ADC(2)	0.928	1.631	1.356	1.682
	COSMO-ADC(2)	1.999	2.001	2.219	2.129
	CC2	1.953	1.989	2.178	2.102

energies with ADC(2) and CC2 in combination with COSMO, the post-SCF coupling scheme was used, as first introduced in ref 85 for the polarizable embedding model and later also combined with COSMO and compared in ref 86 to other reaction field coupling schemes. The notation A//B refers to an electronic excitation energy computed at a level A using a geometry optimized at a level B. For visualization of electronic excitations, natural transition orbitals (NTOs) were plotted at contour values of −0.05 (red) and +0.05 (blue). Further details on the individual calculations, e.g., the basis sets, are given below and in the Supporting Information. All structures together with their Hartree−Fock energies are available from ref 87.

For the calculation of pK_a, initial conformer searches were done to account for the conformational flexibility of the studied photoacids. This was taken care of by using COSMO*conf* (version 2021)[88] in combination with its BP-TZVPD-FINE-COSMO+GAS_18 template. Additional information on the results from the conformer search is given in the Supporting Information (see Tables S1 and S2). The full sets of conformers for both the protonated and deprotonated species of the photoacids were used for the calculation of pK_a, while only a single conformer was considered for the electronic excitation energies since the later are insensitive to conformational changes in the substituents at the sulfonate groups. COSMO-RS as implemented in COSMO*therm* (version 2021)[89] was used to calculate pK_a in DMSO and water at the BP-TZVP and BP-TZVPD-FINE levels of theory (e.g., see ref 90 for further details). The main difference between these two is that the latter uses refined energies calculated in the larger def2-TZVPD basis set and with a smooth radii-based isosurface for COSMO.[91] At its core, COSMO*therm* uses a linear free-energy relationship (LFER) between pK_a and the calculated Gibbs free energy difference in solution (soln.) between RO^- and ROH, obtained with COSMO-RS,

$$pK_a = a + b(G_{soln.}(RO^-) - G_{soln.}(ROH)) \quad (2)$$

where a and b are the implemented LFER parameters that were originally derived from a linear fit to experimental pK_a values in the given solvent.[89] $G_{soln.}(RO^-)$ and $G_{soln.}(ROH)$ were calculated according to the procedure described in refs 45−48. All calculations involving pK_a refer to a temperature T of 298.15 K (25 °C).

For investigating the importance of the ground-state singles amplitudes, i.e., the difference between MP2 or ADC(2) and CC2, and the role of direct and indirect solvent effects via the molecular structure on the lowest excitation energy, we performed a series of calculations on the protonated and deprotonated forms of compound **F** (compare Scheme 2). The ground-state geometries were optimized in the cc-pVDZ basis set[92,93] using MP2[94,95] or CC2[96] for the gas phase and in combination with COSMO, COSMO-MP2[97] and COSMO-CC2,[98] also for the solution phase. Similarly, the geometries for the first excited state were optimized in the cc-pVDZ basis set using ADC(2)[96] and CC2[99] for the gas phase and COSMO-ADC(2)[98] for the solution phase. The vertical electronic excitation energies were calculated in the larger aug-cc-pVDZ basis set[93,100] at the gas-phase ADC(2)[101] and CC2[102] as well as solution-phase COSMO-ADC(2)[98] and COSMO-CC2[98] levels. COSMO-CC2//COSMO-ADC(2) excitation energies for the excited state are used as estimates for the COSMO-CC2//COSMO-CC2 results. The obtained excitation energies for the first vertical transitions are given in Table 1.

METHOD VALIDATION

Prior to a systematic study on the whole set of Jung's photoacids, we extensively tested our selected methods on the protonated (acid) and deprotonated (base) forms of compound **F** (cmp. Scheme 2). We studied the convergence of the ground-state geometries with the methods and basis sets, the convergence of the electronic excitation energies with the basis-set size, and the difference between ADC(2) and CC2 excitation energies. The corresponding results and further computational details are given in the Supporting Information, and only the main aspects will be briefly summarized here.

Convergence of the Excitation Energies with the Ground-State Geometries and Basis Sets. Geometry optimizations with different DFT functionals and MP2 with different basis sets (see Table S3) show that the method for the ground-state structure has only a small effect (≤0.1 eV) on the ADC(2)/aug-cc-pVDZ excitation energies. We thus decided to

https://doi.org/10.1021/acs.jpca.2c04436
J. Phys. Chem. A XXXX, XXX, XXX−XXX

use—if nothing else is stated—MP2/cc-pVDZ as the method for the geometry optimizations because of two reasons: First, MP2 for the ground state will allow for a consistent description with ADC(2) for the excited-state later on. Second, when treating electronically excited states, we will be restricted to smaller basis sets such as cc-pVDZ due to the computational costs of the excited-state geometry optimizations.

We then compared the ADC(2) excitation energies for the first five vertical transitions in different basis sets (see Table S4). Based on the results, we chose the aug-cc-pVDZ basis as a compromise between accuracy and computational costs. The excitation energies for the lowest excited states obtained with this basis set deviate from the results in the aug-cc-pVQZ basis by ≈0.04 eV for the acid and by ≈0.03 eV for the base, which is considerably smaller than the methodical error of ≈0.1 eV for ADC(2) and CC2 (for S_1 in organic chromophores with single-reference ground states relative to the Full-CI limit). Besides, not the absolute excitation energies, but the acid−base energy difference will be of interest for the excited-state pK_a prediction (*vide infra*). Here, we observe a difference between aug-cc-pVDZ and aug-cc-pVQZ for the acid−base difference of only 7 meV, which is probably an order of magnitude smaller than the error due to the electronic structure method and the solvation treatment. According to eq 1, such an error of less than 10 meV in excitation energy corresponds to an error of only 0.17 pK_a units.

With ADC(2)/aug-cc-pVDZ for electronic excitation energies and MP2/cc-pVDZ for the geometry optimizations, we thus use a combination of closely related methods and basis sets. Moreover, aiming at a comparison of calculated and experimental spectra (*vide infra*), other sources of error, in particular regarding the solvation treatment, arise in any case and are expected to be larger than the remaining basis set errors.

Difference between ADC(2) and CC2 Excitation Energies. It turned out that for the lowest excited state in the pyranine-based photoacids the differences between ADC(2) and CC2 are not completely negligible. For the acid, a systematic blue shift of the CC2 compared to the ADC(2) excitation energies at identical geometries is observed. This shift is at the S_0 equilibrium structure in the gas phase about 60 meV and between 40 and 60 meV in solution. At the S_1 equilibrium structure, the differences are larger, between 80 and 110 meV (compare with Table 1). The largest difference between CC2 and ADC(2) is found at the COSMO-ADC(2) geometry for S_1, amounting to about 110 meV.

Also the differences in the equilibrium structures obtained with CC2 and MP2 (S_0) or ADC(2) (S_1) affect the excitation energies, as can be seen by comparing excitation energies for the same method but different geometries (columns in Table 1). The excitation energies obtained at the MP2 and COSMO-MP2 structures for S_0 are 35−60 meV higher compared to those at CC2 and COSMO-CC2. For the gas-phase S_1 equilibrium structures, this deviation is much smaller (≤10 meV) with almost coinciding excitation energies. Since excited-state gradients for COSMO-CC2 are not available, we could not optimize the S_1 structure at this level. The above result, however, gives us reason to assume that the corresponding excited-state structures in solution will be similar as well and hence that COSMO-CC2 excitation energies at the COSMO-ADC(2) geometries will be a good approximation for the COSMO-CC2 excitation energies at the COSMO-CC2 S_1 structure.

For the base, similar results are obtained, i.e.,

- a systematic, but considerably larger blue shift of CC2 vs ADC(2): ≈ 190 meV (gas phase) and ≈110 eV (solution phase) for S_0 and >200 meV (gas phase) and >110 meV (solution phase) for S_1;
- only minor differences between the excitation energies at the MP2 and CC2 ground-state geometries of only ≈20 meV (gas phase) and 20−30 meV (solution phase).

However, there are also distinct differences between the spectroscopic properties of the acid and the base. ADC(2) fails for the excited-state geometry optimization of the base in the gas phase, yielding a nonphysically small excitation energy in the near-infrared region (≫ 800 nm). Interestingly, this issue does not seem to occur in solution, i.e., in combination with COSMO. The COSMO-ADC(2) geometry results in excitation energies that are close to that for the CC2 equilibrium structure. The ADC(2) failure for the excited state in the gas phase is presumably related to the negative charge of the base, on which the solvent has a significant stabilizing effect. The main issue with ADC(2) in the gas phase seems to be a different order of the excited states in the different media: In the gas phase, the first excitation is no longer a HOMO−LUMO (*vide infra*) but a HOMO-3−LUMO transition, which occurs in solution only as the third excitation.

The general deviations between ADC(2) and CC2 excitation energies observed here for photoacid **F** are mainly due to missing contributions in the description of the electronic ground state for ADC(2) which is described as for MP2 using the first-order correction (MP1) to the wave function, including only double excitations out of the (closed-shell) Hartree−Fock reference determinant. Contributions from singly excited determinants to the ground state are missing. For the pyranine derivatives, the single excitation from the HOMO to the LUMO makes, however, a contribution to the correlated ground-state that is not completely negligible, which can be tested by checking the natural transition orbitals (NTOs) generated from the (ground-state) CC2 T_1 amplitudes (see Figure S1). For both the acid and base, the dominant NTO pair resembles that for the first excitation, S_1, especially the virtual NTO, indicating that these orbitals are already partially occupied in the ground state. Moreover, the weights of these NTOs are slightly larger for the base (14.2%) compared to the acid (11.3%); i.e., the need for the singles contribution for an accurate description of the ground state is more pronounced for the base. The neglect of these contributions in ADC(2) leads to an underestimation of the excitation energy for S_1.

SOLVENT EFFECTS: DISENTANGLING ENERGETIC AND STRUCTURAL CONTRIBUTIONS TO THE EXCITATION ENERGIES

After having selected MP2/cc-pVDZ for the ground-state geometries and ADC(2)/aug-cc-pVDZ for excitation energies for our purposes, we turn our focus on the structural and energetic solvent contributions to the excitation energies of the protonated and deprotonated species of photoacid **F**.

Limitations of Continuum Solvation with COSMO. In general, the COSMO-related error in excitation energies typically varies over a broad range, depending on the polarity and proticity of the solvent. For the combinations of COSMO with ADC(2) or CC2 based on the post-SCF coupling scheme, we expect errors compared to experimental data of 0.05−0.07 eV in DMSO based on the reported errors in solvatochromic shifts in water and acetonitrile.[86] This error is significantly larger

https://doi.org/10.1021/acs.jpca.2c04436
J. Phys. Chem. A XXXX, XXX, XXX−XXX

than the remaining basis set contributions and could amount to up to one pK_a unit. While the COSMO error is generally larger for protic—and at the same time often strongly polar—solvents due to the lack of describing H-bond interactions between the solute and the solvent, the accuracy of COSMO is also for nonpolar solvents limited by the neglect of London dispersion and Pauli repulsion interactions. DMSO, as a polar and aprotic solvent, thus appears to be a suitable solvent for COSMO, with only the H-bond acceptance of the solvent missing in the description. Since DMSO is no significant H-bond donor, we expect the largest explicit solvation effects via specific interactions on the protonated, rather than the deprotonated species.

Stokes and Solvatochromic Shifts of the Acid. The Stokes shift, i.e., the difference in absorption and fluorescence emission energies of a given species, is of particular importance for photoacidity. Calculated absorption and emission energies refer to excitation energies at the ground-state (S_0) and excited-state (S_1) equilibrium geometries. From a comparison of the absorption and emission energies in Table 1, we obtain for the Stokes shifts values of 343 meV for ADC(2) and 278 meV for CC2 in the gas phase and, respectively, 410 and 303 meV in the solution phase. Hence, the Stokes shift of the acid appears to be larger in solution, but overall smaller for CC2.

Another interesting aspect are solvatochromic effects which can be determined from the gas-phase and solution-phase absorption and emission energies (diagonal elements of each S_0 and S_1 block in Table 1). Whereas bathochromic, i.e., solvatochromic red shifts of 151 and 172 meV are obtained for the vertical excitation energies at the ground-state structures for ADC(2) and CC2, respectively, the solvatochromic shifts are larger for the vertical transition energies at the excited-state structure rising to 218 and 197 meV. This finding is in accordance with a strong charge redistribution upon excitation of the photoacid, which increases the polarity (*vide infra*).

To separate structural and energetic effects on the excitation energy, we can compare COSMO-ADC(2)//MP2 (2.975 eV) with COSMO-ADC(2)//COSMO-MP2 (2.957 eV) energies which demonstrate that the ground-state solvatochromism is mainly due to a purely energetic effect on the excitation energy itself, rather than a structural effect. Only 18 meV are missing referring to the value in solution if the COSMO-ADC(2) excitation energy is calculated at the MP2 gas-phase geometry. Similar results are obtained for CC2: also COSMO-CC2//CC2 (2.975 eV) differs from COSMO-CC2//COSMO-CC2 (2.958 eV) by only 17 meV. For the excited-state solvatochromism, the largest contribution is again due to direct energetic effects, but the difference between COSMO-ADC(2)//ADC(2) and COSMO-ADC(2)//COSMO-ADC(2) is comparably larger (55 meV).

Stokes and Solvatochromic Shifts of the Base. For the base, the results for the Stokes shifts are in the gas phase 151 meV for CC2 and in the solution phase 173 meV for ADC(2) and 124 meV for CC2. For the solvatochromic shifts, we obtained −3 meV with ADC(2) and +76 meV with CC2 for the vertical transition at the ground-state structure and 49 meV with CC2 for the vertical transition at the excited-state equilibrium structure. The unreliable ADC(2) excited-state geometry prevents an analysis of structural similarities, Stokes shifts, and solvatochromic shifts for ADC(2) as consistently is done above for the acid. As a replacement for the ADC(2)//ADC(2) energy, either the ADC(2)//CC2 result, assuming structural similarities between the methods, or the ADC(2)//COSMO-ADC(2) result, assuming negligible solvent effects on the structures, could be used. Using the former result, as supported by the smaller energy deviation observed for excited-state acid, we can estimate the ADC(2) gas-phase Stokes shift to be 218 meV and the excited-state solvatochromic shift to be −48 meV. The Stokes shift hence again appears to be smaller in solution compared to the gas phase and smaller for CC2 compared to ADC(2), as observed for the acid.

Furthermore, both the ground-state and excited-state solvatochromism of the base do not show a clear trend at these levels since the shift is bathochromic for CC2, but hypsochromic for ADC(2). Still, both results are much smaller in magnitude compared to the acid, indicating that the polarity difference between the ground and excited state seems either less pronounced or even reversed. This is in accordance with the experiments where bathochromic shifts are observed for the protonated as well as methylated photoacids, whereas pronounced hypsochromic shifts are observed for the deprotonated species.[15] This bathochromism is furthermore known to increase linearly as a function of the Kamlet−Taft dipolarity and polarizability parameter π^*, while this hypsochromism increases as a function of the Kamlet−Taft parameter α for the hydrogen-bond donating ability of the solvent. While the latter is not well described by COSMO as it is a pure continuum solvation model, its effect in DMSO is still considered negligible due to the lacking H-bond donating ability ($\alpha = 0$).[15] Rather, H-bonding interactions between the protonated photoacid acting as the donor and DMSO acting as the acceptor are anticipated to have a somewhat larger effect, e.g., as judged based on the large Kamlet−Taft H-bond accepting ability β for DMSO (0.76),[15] although the correlation of excited-state acidity with β is experimentally found to be less indicative compared to that for π^*.

Moreover, as for the acid also for the base, the solvent does not seem to affect the ground-state geometries significantly because the ADC(2) and CC2 energies (i.e., without COSMO) are almost identical at the equilibrium structures for the gas and the solution phase. Calculating solution-phase excitation energies at the corresponding gas-phase geometries, we obtain residuals of −40 meV (COSMO-ADC(2)//MP2) and 24 meV (COSMO-CC2//CC2), as well as −12 meV (COSMO-ADC(2)//ADC(2)) and 49 meV (COSMO-CC2//CC2) referring to the results at the actual ground-state and excited-state structures in solution, respectively.

These results show that (i) the solvent, as described by an implicit model, only has a minor effect on the molecular structure; (ii) the difference between the ADC(2) and CC2 result for the lowest energy is considerably larger for the base; (iii) ADC(2) fails in the excited-state geometry optimization for the base in the gas phase; and (iv) acid and base appear to have a different solvatochromic behavior.

UV/VIS ABSORPTION AND FLUORESCENCE EMISSION SPECTRA

For a systematic study of Jung's photoacids and a comparison with the available experimental UV/Vis absorption and fluorescence emission spectra in DMSO, we did geometry optimizations in the cc-pVDZ basis set using COSMO-MP2 for the ground state and COSMO-ADC(2) for the first excited state. Ground-state structures were used for calculating the UV/Vis absorption spectra and excited-state structures for the fluorescence emission spectra. These calculations were done in solution phase using COSMO for the solvent DMSO. Because

https://doi.org/10.1021/acs.jpca.2c04436
J. Phys. Chem. A XXXX, XXX, XXX−XXX

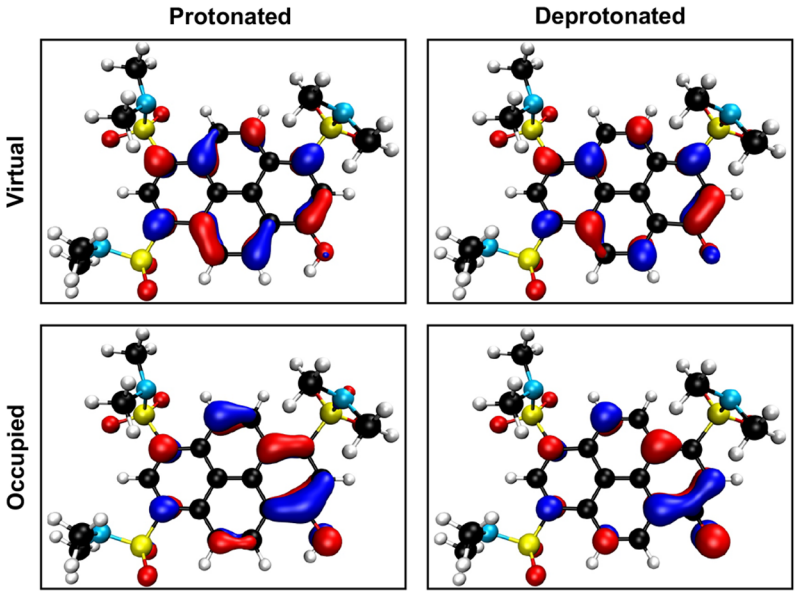


Figure 1. Comparison of the occupied and virtual NTOs for the first NTO pair of the first vertical electronic transition of the protonated and deprotonated species of photoacid **F**. Excitations are calculated with COSMO-ADC(2)/aug-cc-pVDZ at the COSMO-MP2/cc-pVDZ geometries, plotted at contour values of ±0.05 au. The weights of these NTOs are 97.4% (protonated) and 98.0% (deprotonated), respectively.

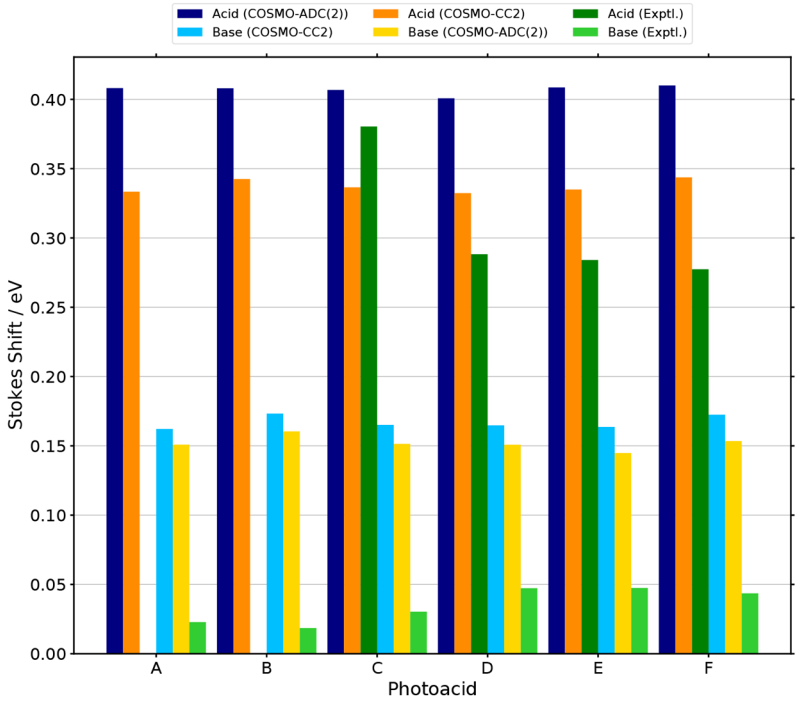


Figure 2. Comparison of calculated and experimental Stokes shifts of the acid and base forms of the photoacids **A**–**F** in the solvent DMSO. Stokes shifts based on the calculated absorption and emission energies of the first vertical transition at the COSMO-ADC(2) and COSMO-CC2 levels (cf. Table S9) as well as for the experimental values taken from ref 14. The corresponding numerical values of the Stokes shifts are given in Table S10.

no implementation of COSMO-CC2 excited-state gradients is yet available, COSMO-CC2 emission energies were estimated based on COSMO-CC2 excitation energies at the COSMO-ADC(2) geometries. All spectra, i.e., electronic excitation energies and oscillator strengths, were computed with COSMO-ADC(2) as well as with COSMO-CC2.

Character of the First Excitation. The first vertical electronic transition is most relevant since it defines the reference for comparison with experimental absorption ($S_0 \rightarrow S_1$) and emission ($S_1 \rightarrow S_0$). The corresponding natural transition orbitals (NTOs) relating to the first transition are exemplarily shown in Figure 1 for the protonated and deprotonated species of photoacid **F**. A full review of the NTOs for the first five vertical transitions of photoacid **F** is given in Tables S5 and S6 of the Supporting Information.

As can be seen in Figure 1, the first transition has for both species $\pi \rightarrow \pi^*$ character, which is typical for aromatic molecules. Moreover, comparison with the molecular orbitals

https://doi.org/10.1021/acs.jpca.2c04436
J. Phys. Chem. A XXXX, XXX, XXX−XXX

revealed that these two excitations represent simple HOMO−LUMO transitions. The additional lone pair and larger negative charge at the O atom in the deprotonated species lead to a larger contribution from the p orbital at the O atom to the occupied NTO compared to the protonated form. Plots for the electron density difference between S_1 and S_0 (see Figure S2, SI) show that this electronic transition is associated with a large charge redistribution, i.e., an intramolecular charge transfer (ICT) which reduces the electron density at the −OH or $-O^-$ group, shifting it toward the electron-pulling sulfonic acid groups.

Due to the structural similarity, the character of the electronic transitions is basically identical for all pyranine derivatives studied here and, especially, the most relevant first transition remains unaltered, as verified by NTO analysis. For further reference, the NTOs for the first vertical transition of the protonated and deprotonated species of the photoacids **A**−**F** are shown in Tabs. S7 and S8. In particular, this first transition was always found to be bright, i.e., to have nonzero oscillator strengths. Therefore, it is sufficient to simply restrict the discussion to the excitation energies for this transition. The corresponding (de)excitation energies for the acid and base forms of the six photoacids **A**−**F** are listed in Table S9, at the two levels of theory and together with their experimental values.

Comparison of Stokes and Substitution Shifts. The direct comparison of the calculated absorption and emission energies in Table S9 to their experimental counterparts is significantly affected by the systematic errors arising from the limitations of the computational approach (*vide supra*). This includes the restriction to the second-order methods ADC(2) and CC2 and to purely electrostatic solute−solvent interactions, and importantly, that the experimental values refer to maximum positions in the experimental spectra, whereas the calculated results are vertical (de)excitation energies. In short, such a direct comparison reflects that the overall performance is largely affected by an error cancellation involving the inherent errors or ADC(2) or CC2, the (missing) solvation contributions, and the underestimation of fluorescence energies. As a result, best agreements between the calculated and experimental values are found for the emission energies of the acids and the absorption energies of the bases, both at the COSMO-CC2 level. In contrast, the absorption energies of the acids are systematically overestimated (≤0.15 eV), while the emission energies of the bases are underestimated (≤0.10 eV). Still, these errors appear to benefit from further compensation when including explicit solvent due to the experimentally observed solvatochromism, i.e., the bathochromic and hypsochromic behavior of the acid and base, respectively (*vide infra*).

To minimize the effect of systematic shifts, the comparison of relative energies is much more reasonable instead. One such quantity is the Stokes shift (see Figure 2 or Table S10). The results show that ADC(2) and CC2 both overestimate the Stokes shifts for the acids as well as for the bases: CC2 by 40−70 meV for the acids and 100−140 meV for the bases, ADC(2) by 110−130 meV for the acids and 120−150 meV for bases. One exception is photoacid **C**, where the experimental Stokes shift is between the CC2 and ADC(2) values. That the calculated results overestimate the experimental Stokes shifts might partially be due to the vertical approximation but, in particular for the bases, also due to the approximations in the COSMO solvation model.

The substitution shifts in Table 2 demonstrate an overall better performance of COSMO-CC2 over COSMO-ADC(2). In particular, almost quantitative agreement between the calculated and experimental results is obtained for the relative order of the absorption energies for the acids, with the exception of photoacid **D**. The calculated trends for the absorption energies of the bases are in good agreement with the experiments; only for the photoacids **B** and **D** the substutional shifts relative to **F** are overestimated somewhat. However, the deviations are in the order of only a few hundredths of an eV.

Table 2. Substitutional Shifts in the UV/Vis Absorption and Fluorescence Emission Energies of Jungs's Photoacids in the Solvent DMSO[a]

		photoacids					
	level	**A**	**B**	**C**	**D**	**E**	**F**
				acid			
S_0	COSMO-ADC(2)	−72	−139	−56	−87	6	0
	COSMO-CC2	−61	−117	−53	−78	7	0
	experiment	−59	−115	−46	0	7	0
S_1	COSMO-ADC(2)	−70	−137	−53	−77	8	0
	COSMO-CC2	−50	−116	−45	−66	16	0
	experiment	—	—	−149	−11	0	0
				base			
S_0	COSMO-ADC(2)	−68	−150	−72	−67	15	0
	COSMO-CC2	−54	−127	−63	−53	17	0
	Experiment	−55	−85	−55	−4	0	0
S_1	COSMO-ADC(2)	−58	−151	−65	−60	24	0
	COSMO-CC2	−52	−134	−61	−51	26	0
	experiment	−34	−60	−42	−8	−4	0

[a]Comparison of differences in the vertical electronic excitation energies for the first transition taken from the calculations (cf. Table S9) and experimental results (from ref 14) of the photoacids **A**−**F** relative to photoacid **F**. Values are given in meV.

Due to nearly quantitative ESPT yield in DMSO, no experimental emission energies are available for the protonated species of photoacids **A** and **B**.[14] For the remaining photoacids, no clear difference between the results for the two species can be observed due to the reduced number of reference values. However, the deviations from the experimental shifts between the different substituents appear to be larger in emission compared to absorption. The underestimation of fluorescence emission energies is commonly known and originates from the discrepancy between the excited-state equilibrium structures used for the vertical approximation and those actually leading to the emission band maxima in experiments. In contrast to UV/Vis absorption spectroscopy, where the initial state is well-defined, the choice of the initial state in fluorescence is less clear. This is because the fluorescence (i.e., the radiative transition from the electronically excited state, usually S_1, to the electronic ground state) can take place at any geometry after vertical excitation, i.e., any structure in between the Franck−Condon point and the excited-state equilibrium. Also, the computational results for excited-state potential surfaces have larger uncertainties than for the ground-state surfaces.[103]

An important factor for the Stokes shift is the change in the equilibrium structure from the ground to the electronically excited state due to changes in the electronic structure. The larger Stokes shifts of the acids observed for the pyranine derivatives indicate stronger structural changes after electronic excitation which can be rationalized in terms of (anti)-aromaticity, as reviewed, e.g., by Agmon[23] or recently Wen et al.:[104] ROH is more aromatic compared to RO^- in S_0 and, thus, experiences a larger loss in aromaticity upon excitation to S_1. As a consequence, the structural changes in the aromatic system from

https://doi.org/10.1021/acs.jpca.2c04436
J. Phys. Chem. A XXXX, XXX, XXX−XXX

Table 3. Comparison of Calculated Ground-State and Excited-State Acidities of the Photoacids A−F in the Solvent DMSO[a]

		photoacids					
	level	A	B	C	D	E	F
pK_a	COSMO-RS	4.8 (3.2)	3.9 (3.5)	6.5 (4.9)	7.9 (5.0)	6.9 (6.4)	7.2 (6.0)
				absorption			
ΔpK_a	COSMO-ADC(2)	−13.2	−13.4	−13.5	−12.9	−13.1	−13.2
	COSMO-CC2	−12.0	−12.3	−12.3	−11.7	−11.9	−12.1
	experimental	−10.7	−10.3	−11.0	−10.9	−10.9	−10.8
				emission			
ΔpK_a	COSMO-ADC(2)	−9.0	−9.5	−9.4	−8.9	−8.9	−9.2
	COSMO-CC2	−8.9	−9.2	−9.2	−8.6	−8.7	−8.9
	experimental	—	—	−5.0	−6.8	−6.9	−6.8
				averaged			
ΔpK_a	COSMO-ADC(2)	−11.1	−11.4	−11.5	−10.9	−11.0	−11.2
	COSMO-CC2	−10.4	−10.7	−10.7	−10.2	−10.3	−10.5
	experimental	—	—	−8.0	−8.8	−8.9	−8.8
				averaged			
pK_a^*	COSMO-ADC(2)	−6.3 (−7.9)	−7.5 (−7.9)	−5.0 (−6.6)	−3.0 (−5.9)	−4.1 (−4.7)	−4.0 (−5.2)
	COSMO-CC2	−5.7 (−7.3)	−6.8 (−7.2)	−4.3 (−5.9)	−2.2 (−5.1)	−3.4 (−4.0)	−3.3 (−4.5)

[a] pK_a values using COSMO-RS at the BP-TZVP (BP-TZVPD-FINE) level. ΔpK_a based on the Förster cycle using either the absorption, emission, or averaged excitation energies at the COSMO-ADC(2), COSMO-CC2, and experimental levels. pK_a^* using the BP-TZVP (BP-TZVPD-FINE) pK_a and the averaged Förster cycle ΔpK_a values at the two levels COSMO-ADC(2) and COSMO-CC2. Experimental results are calculated based on ref 14, with no data for pK_a^* due to missing experimental ground-state pK_a in DMSO.

S_0 to S_1 are larger. This observation is also confirmed by the root-mean-square deviation for the C−C bond lengths in the pyrene ring between the S_1 and S_0 structures, e.g., 2.2 pm for the acid and 1.1 pm for the base of photoacid **F**.

PREDICTION OF pK_A^* IN DMSO

The calculated absorption and emission energies were used to compute ΔpK_a values for Jung's photoacids based on the Förster cycle, according to

$$\Delta pK_a = pK_a^* - pK_a = \frac{\Delta G_{exci}(RO^-) - \Delta G_{exci}(ROH)}{RT\ \ln(10)} \quad (3)$$

and pK_a^* values (via eq 1) using the pK_a, calculated as described in the Computational Details section. The results for pK_a, ΔpK_a, and pK_a^* of the six photoacids in the solvent DMSO are summarized in Table 3.

Ground-State Acidity. Since no experimental pK_a values are available for the photoacids **A**−**F** in DMSO, we additionally calculated the corresponding values in water (see Table S11), where experimental reference data for a comparison is available. The results in water demonstrate that the pK_a values calculated at the BP-TZVP level of COSMO-RS are in much better agreement with the experimental values than the BP-TZVPD-FINE results, based on mean absolute errors of 0.4 and 0.8, respectively. In particular, the BP-TZVPD-FINE results are qualitatively wrong for the differences in acidity between the compounds **A**−**F**. This lead us to infer that the performance of BP-TZVP will be also better in the solvent DMSO.

Regarding the pK_a values at the BP-TZVP level in DMSO (Table 3), a similar order of acidity as in water can be observed: Photoacid **B** is predicted to be most acidic (3.9) but close to **A** (4.8), whereas **D** (7.9) is least acidic, and **C**, **E**, and **F** have comparable acidities.

Acidity Increase Upon Photoexcitation. Computing ΔpK_a, i.e. the change in pK_a upon excitation into S_1, via the Förster cycle does not require the ground-state pK_a values and could therefore be done with the experimental as well as the calculated absorption and emission energies. Moreover, also averaged ΔpK_a values using the mean absorption and emission energies were considered since these are frequently used in the experimental pK_a^* determination. These mean energies represent an approximation to the true 0−0 transition energies that should be ideally inserted into the Förster equation. This implicitly assumes that the shapes (i.e., curvature) of the potential energy surfaces in the electronic ground and excited states are similar, so that the vibrational contributions to the vibronic 0−0 transition can effectively cancel out in the average.

Being based on the excitation energies in Table S9, the calculated ΔpK_a values reflect the trends and deviations that were discussed before. In detail, the trends in the excitation energies explain that (i) ΔpK_a is larger when calculated from absorption energies compared to the results obtained from the emission energies for both the theoretical and the experimental results, as rationalized by the Stokes shifts; (ii) the difference between the results for COSMO-ADC(2) and COSMO-CC2 is larger for absorption (≈ 1.2) compared to emission (≈ 0.2); and (iii) the difference between the calculated and experimental values is again smaller for absorption compared to emission (e.g., for COSMO-CC2, 1.3 and 2.9, respectively).

Considering the relative order of ΔpK_a at a specific level, we observe that the studied photoacids basically reveal the same experimental ΔpK_a in absorption (of approximately −11), largest for **C** and smallest for **B**. Similarly, this observations also holds for the calculated results, but with larger fluctuations and a noticeably overestimated result for photoacid **B**. In contrast, the experimental ΔpK_a in emission reveals a distinct difference between photoacid **C** and photoacids **D**−**F**, which cannot be reproduced by the calculations. Photoacid **E** gives the largest experimental ΔpK_a, whereas it is again photoacid **B** in the calculations.

Solvent Comparison and Origin of Photoacidity. Due to the missing experimental emission energies for the acid forms of **A** and **B** in the solvent DMSO (cf. Table 2), no experimental ΔpK_a for emission and thus also no averaged values are available for these two compounds. Consequently, comparing the

https://doi.org/10.1021/acs.jpca.2c04436
J. Phys. Chem. A XXXX, XXX, XXX−XXX

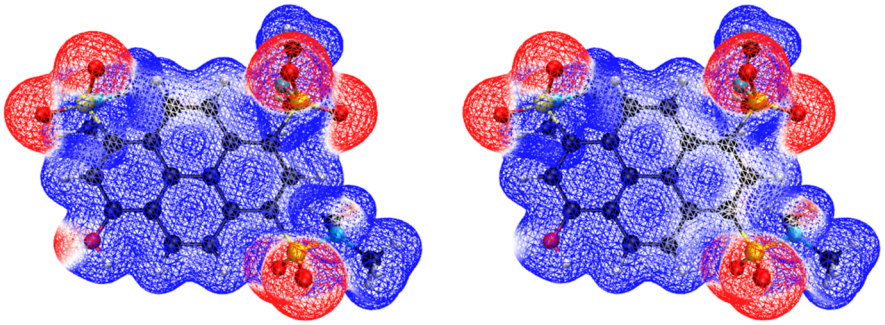


Figure 3. Electrostatic potential plotted in the range from −0.03 (red) to 0.03 (blue) [au] at the electron density isosurface (contour value: 0.01 au) of the electronic ground state S_0 (a) and excited state S_1 (b) of the protonated species of photoacid **F** in solution. Densities calculated at COSMO-MP2 for S_0 and COSMO-ADC(2) for S_1 in the aug-cc-pVDZ basis set using the COSMO-MP2/cc-pVDZ solution-phase geometry. The molecule is oriented such that the −OH group is located on the bottom left with the H atom pointing to the lower right.

averaged ΔpK_a is only of limited use in the special case of these photoacids. On the contrary, all of these results are known in water (see Table S11), allowing for a comparison of the two solvents. In water, the averaged experimental acidity change is smallest in magnitude for photoacids **D**−**F** (ca. − 6.5), slightly increases via **C** (− 6.8) and **A** (− 7.4), and reaches its maximum at **B** (− 8.3). A similar trend is found for our calculated averaged ΔpK_a values, but photoacids **B** and **C** are predicted to have the largest and most comparable changes. However, whereas the experimental ΔpK_a of photoacid **B** in water is dominated by the absorption contribution, the respective contributions in DMSO are quite similar for all photoacids studied here, as proven by both calculations and experiments.

Despite these slight deviations in the order of the photoacidity, the overall difference between the series for the two solvents allows for an interesting observation on its own: ΔpK_a is generally smaller in water, i.e., in the more polar solvent, compared to DMSO, the less polar solvent. This finding is supported by both the experimental and the calculated spectra and it can be rationalized on a simplified level by considering the solvent effects on each of the four species in the Förster cycle (cf. Scheme 1). Due to an intramolecular charge transfer (ICT) upon excitation, ROH* is more polar than ROH and hence stabilized more strongly by a polar solvent. This polarity change is exemplarily illustrated in Figure 3 for ROH and ROH* of photoacid **F** using the electrostatic potential. In analogy, the strong polarity of the RO^- anion is reduced by a similar ICT, which causes RO^-* to be less polar (see Figure S3) and hence less strongly stabilized compared to RO^-.

This implies that ROH reveals a bathochromic and RO^- a (more) hypsochromic shift, as indeed also observed in experiments. Moreover, the ΔpK_a is actually dominated by the energy gap between ROH* and RO^- because both ROH and RO^-* are rather nonpolar. However, since RO^- is an anion, its stabilization by a polar solvent is larger than that of the charge-neutral ROH* species, and thus ΔpK_a will decrease in magnitude with increasing solvent polarity. In line with this, the CC2 results for photoacid **F** (cf. Table 1) predict a ΔpK_a in the gas phase of −13.5 (absorption) and −11.4 (emission), i.e., −12.5 on average, which is even considerably more negative than the corresponding result in DMSO (−10.5).

Excited-State Acidity. From the pK_a and ΔpK_a, we computed the pK_a^* values listed in Table 3. For the sake of brevity, only pK_a^* values based on the averaged COSMO-CC2 ΔpK_a in combination with BP-TZVP pK_a are considered. Our calculations predict compound **B** with a pK_a^* of −6.8 to be the strongest photoacid in the solvent DMSO, followed by compounds **A** (−5.7), **C** (−4.3), **E** (−3.4), and **F** (−3.3) toward the weakest photoacid **D** (−2.2). Interestingly, this order exactly matches the one for the experimental Förster cycle pK_a^* values in water.

Whereas in water the photoacids only span a range of three pK_a units, this range is predicted to be larger in DMSO, covering almost five units. This is again due to the solvent effect causing the ΔpK_a contribution to decrease in magnitude with increasing solvent polarity (*vide supra*). However, the pK_a jump upon excitation is comparable for these six structurally related photoacids and it is the ground-state pK_a that decides which of these photoacids is the strongest.

Moreover, our calculations predict negative pK_a^* values for all of these photoacids. Since the pK_a values of any two given compounds (in the same solvent) determine the position of the corresponding proton-transfer equilibrium, the pK_a^* of the photoacid and pK_a of the protonated solvent decide to what extent protonation of the solvent is expected. A comparison with the pK_a value for an isolated protonated DMSO molecule of 2.9 at the BP-TZVP level (or −0.71 at BP-TZVPD-FINE level) or with the ideal value[37] of $-\log[S] = -1.15$ (where $[S] = 14.08$ mol L^{-1} is the solvent concentration[105]) reveals that the pK_a^* values for all six studied photoacids are all considerably more negative. Thus, all six compounds are in the solvent DMSO true superphotoacids; i.e., they will be able to efficiently protonate the solvent.

CONCLUSIONS

This work applied the correlated wavefunction-based methods ADC(2) and CC2 in combination with the implicit solvent model COSMO to the theoretical spectroscopy of Jung's pyranine-derived photoacids in the solvent DMSO. Our calculated UV/Vis absorption and fluorescence emission energies are able to reproduce the experimental trends in the Stokes shifts as well as substitution shifts of the protonated and deprotonated species. In terms of trends, the calculations are typically in better agreement with the experiments for absorption compared to emission energies and for the protonated compared to the deprotonated species. In contrast, regarding absolute absorption and emission energies, we observe that COSMO-CC2 performs particularly better for the ROH emission and RO^- absorption in comparison to ROH absorption and RO^- emission. However, this performance

https://doi.org/10.1021/acs.jpca.2c04436
J. Phys. Chem. A XXXX, XXX, XXX−XXX

should be considered the outcome of some beneficial error cancellation due to the combination of the method, solvation description, and the respective electronic state. An overestimation of the vertical absorption energies in the order of 0.1 eV is within the range of the typical errors observed for the second-order methods ADC(2) and CC2 in benchmarks relative to higher-order wavefunction methods.[106] Probably because of error compensation, the results for 0−0 energies are for these methods typically in better agreement with experiment.[107] For vertical emission energies, the single-reference methods ADC(2) and CC2 have probably a tendency to give too low results because of an overestimation of ground-state energies at distorted structures. For the comparison with band maxima in experimental fluorescence spectra, an additional error source is the assumption that the emission occurs from the fully relaxed excited-state structure at the minimum of the S_1 potential energy surface.

Despite being limited to purely electrostatic interactions, implicit solvent effects as described by COSMO appear to be sufficient for the solvation treatment of these photoacids in DMSO in first order. More precisely, for these photoacids, solvent effects on the electronic excitation energies occur mainly through the energetic contribution itself rather than structural effects on the geometries.

The strong photoacidity of these compounds originates from an intramolecular charge transfer upon electronic excitation from the −OH or $-O^-$ group to the aromatic ring system and the sulfonate groups in both the protonated and deprotonated species, causing the corresponding energy difference between the two species to change in favor of the deprotonated form in the excited state. Eventually, the relative energetic order of these species in the respective electronic states also explains the observed solvent effect: ΔpK_a, the pK_a jump during excitation, decreases with increasing polarity of the solvent due to a stronger stabilization of RO^- relative to ROH*. For ΔpK_a, we found that our calculated averaged results in DMSO are accurate within two pK_a units. Moreover, this quantity serves as an excellent example to illustrate the need for having directly comparable computational and experimental results. For example, the experimental ΔpK_a values based on either absorption or emission energies differ by more than four pK_a units. All studied photoacids are predicted to be actual superphotoacids in DMSO, i.e., to perform an efficient excited-state proton transfer to the solvent owing to negative pK_a^*, with compound **B** being the strongest among them. Careful analysis of the individual contributions to pK_a^* revealed though that the exact order in excited-state acidity of these compounds is controlled by their ground-state pK_a, rather than by ΔpK_a.

As our main difficulties encountered in this study, we identify the limitations due to the vertical approximation used during the calculation of excitation energies, which does not take into account vibronic effects and solvent-dependent broadening, as well as those due to the restriction to an implicit solvent model. Therefore, in order to obtain a better agreement with the experiments, going beyond implicit solvation and performing (*ab initio*) MD simulations with explicit solvent appears necessary. Unfortunately, for the rather large molecules studied here, this is rather difficult from a technical point-of-view, especially for the electronically excited states. These are required since the averaged absorption and fluorescence energies are typically used in the experimental calculation of ΔpK_a, as pointed out before. *Ab initio* MD simulations are practically limited to TDDFT for the electronic structure, not allowing for CC2 MD in solution. Also, the large size of the molecules probably poses another problem because a large simulation box, i.e., a high number of solvent molecules, would be needed to avoid self-interactions in a setup that uses periodic boundary conditions.

■ ASSOCIATED CONTENT

Supporting Information

The Supporting Information is available free of charge at https://pubs.acs.org/doi/10.1021/acs.jpca.2c04436.

Computational details and results for the convergence study of electronic excitation energies with different methods and basis sets; NTOs for the ground-state CC2 T_1 amplitudes, the first five electronic transitions of the acid and base of photoacid F, and the first transition for both species of all six photoacids A−F; plots of the difference electron density of the acid and base in the gas and solution phase; plots of the electrostatic potential of the base in S_0 and S_1; calculated absorption and emission energies of the acid and base of the six photoacids; details on the obtained conformer sets; and calculated pK_a values of the six photoacids in water (PDF)

■ AUTHOR INFORMATION

Corresponding Author

Niklas Sülzner − *Lehrstuhl für Theoretische Chemie, Ruhr-Universität Bochum, 44780 Bochum, Germany;* orcid.org/0000-0002-8734-5807; Phone: +49 (0)234 32-24250; Email: niklas.suelzner@rub.de; Fax: +49 (0)234 32-14045

Author

Christof Hättig − *Lehrstuhl für Theoretische Chemie, Ruhr-Universität Bochum, 44780 Bochum, Germany;* orcid.org/0000-0002-5752-2710

Complete contact information is available at: https://pubs.acs.org/10.1021/acs.jpca.2c04436

Notes

The authors declare no competing financial interest.

■ ACKNOWLEDGMENTS

We acknowledge financial support by the Deutsche Forschungsgemeinschaft through Project Ha 2588/8-1. This work was also funded by the Deutsche Forschungsgemeinschaft (DFG, German Research Foundation) under Germany's Excellence Strategy—EXC 2033−390677874−RESOLV.

■ REFERENCES

(1) Chou, P.-T.; Solntsev, K. M. Photoinduced Proton Transfer in Chemistry and Biology. *J. Phys. Chem. B* **2015**, *119*, 2089.

(2) Kagel, H.; Frohme, M.; Glökler, J. Photoacids in Biochemical Applications. *J. Cell. Biol.* **2018**, *4*, 23−30.

(3) Hammes-Schiffer, S. Virtual Issue on Proton Transfer. *J. Phys. Chem. B* **2021**, *125*, 3725−3726.

(4) Simkovitch, R.; Pines, D.; Agmon, N.; Pines, E.; Huppert, D. Reversible Excited-State Proton Geminate Recombination: Revisited. *J. Phys. Chem. B* **2016**, *120*, 12615−12632.

(5) Genosar, L.; Cohen, B.; Huppert, D. Ultrafast Direct Photoacid−Base Reaction. *J. Phys. Chem. A* **2000**, *104*, 6689−6698.

(6) Awasthi, A. A.; Singh, P. K. Proton Transfer Reaction Dynamics of Pyranine in DMSO/Water Mixtures. *ChemPhysChem* **2018**, *19*, 198−207.

(7) Gajst, O.; Pinto da Silva, L.; Esteves da Silva, J. C. G.; Huppert, D. Excited-State Proton Transfer from the Photoacid 2-Naphthol-8-sulfonate to Acetonitrile/Water Mixtures. *J. Phys. Chem. A* **2018**, *122*, 6166−6175.
(8) Gajst, O.; Pinto da Silva, L.; Esteves da Silva, J. C. G.; Huppert, D. Enhanced Excited-State Proton Transfer via a Mixed Methanol-Water Molecular Bridge of 1-Naphthol-3,6-disulfonate in Methanol−Water Mixtures. *J. Phys. Chem. A* **2019**, *123*, 48−58.
(9) Nandi, N.; Sahu, K. Analysis of Excited State Proton Transfer Dynamics of HPTS in Methanol-Water Mixtures from Time-Resolved Area-Normalised Emission Spectrum (TRANES). *J. Photochem. Photobiol., A* **2019**, *374*, 138−144.
(10) Pérez-Lustres, J. L.; Rodriguez-Prieto, F.; Mosquera, M.; Senyushkina, T. A.; Ernsting, N. P.; Kovalenko, S. A. Ultrafast Proton Transfer to Solvent: Molecularity and Intermediates from Solvation- and Diffusion-Controlled Regimes. *J. Am. Chem. Soc.* **2007**, *129*, 5408−5418.
(11) Solntsev, K. M.; Clower, C. E.; Tolbert, L. M.; Huppert, D. 6-Hydroxyquinoline-N-oxides: A New Class of "Super" Photoacids. *J. Am. Chem. Soc.* **2005**, *127*, 8534−8544.
(12) Simkovitch, R.; Shomer, S.; Gepshtein, R.; Roth, M. E.; Shabat, D.; Huppert, D. Comparison of the Rate of Excited-State Proton Transfer from Photoacids to Alcohols and Water. *J. Photochem. Photobiol., A* **2014**, *277*, 90−101.
(13) Simkovitch, R.; Shomer, S.; Gepshtein, R.; Shabat, D.; Huppert, D. Excited-State Proton Transfer from Quinone-Cyanine 9 to Protic Polar-Solvent Mixtures. *J. Phys. Chem. A* **2014**, *118*, 1832−1840.
(14) Finkler, B.; Spies, C.; Vester, M.; Walte, F.; Omlor, K.; Riemann, I.; Zimmer, M.; Stracke, F.; Gerhards, M.; Jung, G. Highly Photostable "Super"-Photoacids for Ultrasensitive Fluorescence Spectroscopy. *Photochem. Photobiol. Sci.* **2014**, *13*, 548−562.
(15) Spies, C.; Finkler, B.; Acar, N.; Jung, G. Solvatochromism of Pyranine-Derived Photoacids. *Phys. Chem. Chem. Phys.* **2013**, *15*, 19893−19905.
(16) Spies, C.; Shomer, S.; Finkler, B.; Pines, D.; Pines, E.; Jung, G.; Huppert, D. Solvent Dependence of Excited-State Proton Transfer from Pyranine-Derived Photoacids. *Phys. Chem. Chem. Phys.* **2014**, *16*, 9104−9114.
(17) Maus, D.; Grandjean, A.; Jung, G. Toward Magic Photoacids: Proton Transfer in Concentrated Sulfuric Acid. *J. Phys. Chem. A* **2018**, *122*, 9025−9030.
(18) Lee, Y. M.; Park, S.-Y.; Kim, H.; Kim, T. G.; Kwon, O.-H. Photoinduced Strong Acid−Weak Base Reactions in a Polar Aprotic Solvent. *Methods Appl. Fluoresc.* **2016**, *4*, 024004.
(19) Kumpulainen, T.; Bakker, B. H.; Hilbers, M.; Brouwer, A. M. Synthesis and Spectroscopic Characterization of 1,8-Naphthalimide Derived "Super" Photoacids. *J. Phys. Chem. B* **2015**, *119*, 2515−2524.
(20) Kumpulainen, T.; Bakker, B. H.; Brouwer, A. M. Complexes of a Naphthalimide Photoacid with Organic Bases, and their Excited-State Dynamics in Polar Aprotic Organic Solvents. *Phys. Chem. Chem. Phys.* **2015**, *17*, 20715−20724.
(21) Kumpulainen, T.; Rosspeintner, A.; Dereka, B.; Vauthey, E. Influence of Solvent Relaxation on Ultrafast Excited-State Proton Transfer to Solvent. *J. Phys. Chem. Lett.* **2017**, *8*, 4516−4521.
(22) Verma, P.; Rosspeintner, A.; Dereka, B.; Vauthey, E.; Kumpulainen, T. Broadband Fluorescence Reveals Mechanistic Differences in Excited-State Proton Transfer to Protic and Aprotic Solvents. *Chem. Sci.* **2020**, *11*, 7963−7971.
(23) Agmon, N. Elementary Steps in Excited-State Proton Transfer. *J. Phys. Chem. A* **2005**, *109*, 13−35.
(24) Simkovitch, R.; Shomer, S.; Gepshtein, R.; Huppert, D. How Fast Can a Proton-Transfer Reaction Be beyond the Solvent-Control Limit? *J. Phys. Chem. B* **2015**, *119*, 2253−2262.
(25) Solntsev, K. M.; Huppert, D.; Agmon, N. Photochemistry of "Super"-Photoacids. Solvent Effects. *J. Phys. Chem. A* **1999**, *103*, 6984−6997.
(26) Solntsev, K. M.; Huppert, D.; Agmon, N.; Tolbert, L. M. Photochemistry of "Super" Photoacids. 2. Excited-State Proton Transfer in Methanol/Water Mixtures. *J. Phys. Chem. A* **2000**, *104*, 4658−4669.
(27) Clower, C.; Solntsev, K. M.; Kowalik, J.; Tolbert, L. M.; Huppert, D. Photochemistry of "Super" Photoacids. 3. Excited-State Proton Transfer from Perfluoroalkylsulfonyl-Substituted 2-Naphthols. *J. Phys. Chem. A* **2002**, *106*, 3114−3122.
(28) Tolbert, L. M.; Solntsev, K. M. Excited-State Proton Transfer: From Constrained Systems to "Super" Photoacids to Superfast Proton Transfer. *Acc. Chem. Res.* **2002**, *35*, 19−27.
(29) Förster, T. Fluoreszenzspektrum und Wasserstoffionenkonzentration. *Naturwissenschaften* **1949**, *36*, 186−187.
(30) Förster, T. Elektrolytische dissoziation angeregter Moleküle. *Z. Elektrochem. Angew. Phys. Chem.* **1950**, *54*, 42−46.
(31) Barcza, L.; Buvári-Barcza, Á. Acid-Base Titrations in Nonaqueous Solvents and Solvent Mixtures. *J. Chem. Educ.* **2003**, *80*, 822.
(32) Buvári-Barcza, A.; Barcza, L. Problems in the Interpretation of Nonaqueous Titrations. *Die Pharmazie* **2005**, *60*, 243−246.
(33) Sooväli, L.; Kaljurand, I.; Kütt, A.; Leito, I. Uncertainty Estimation in Measurement of pKa Values in Nonaqueous Media: A Case Study on Basicity Scale in Acetonitrile Medium. *Anal. Chim. Acta* **2006**, *566*, 290−303.
(34) Alongi, K. S.; Shields, G. C. In *Annual Reports in Computational Chemistry*; Wheeler, R. A., Ed.; Elsevier: 2010; Vol. *6*; pp 113−138.
(35) Seybold, P. G.; Shields, G. C. Computational Estimation of pKa Values. *Wiley Interdiscip. Rev. Comput. Mol. Sci.* **2015**, *5*, 290−297.
(36) Casasnovas, R.; Ortega-Castro, J.; Frau, J.; Donoso, J.; Muñoz, F. Theoretical pKa Calculations with Continuum Model Solvents, Alternative Protocols to Thermodynamic Cycles. *Int. J. Quantum Chem.* **2014**, *114*, 1350−1363.
(37) Pliego, J. R. Thermodynamic Cycles and the Calculation of pKa. *Chem. Phys. Lett.* **2003**, *367*, 145−149.
(38) Klamt, A. Conductor-like Screening Model for Real Solvents: A New Approach to the Quantitative Calculation of Solvation Phenomena. *J. Phys. Chem.* **1995**, *99*, 2224−2235.
(39) Klamt, A.; Jonas, V.; Bürger, T.; Lohrenz, J. C. Refinement and Parametrization of COSMO-RS. *J. Phys. Chem. A* **1998**, *102*, 5074−5085.
(40) Eckert, F.; Klamt, A. Fast Solvent Screening via Quantum Chemistry: COSMO-RS Approach. *AIChE J.* **2002**, *48*, 369−385.
(41) Klamt, A.; Eckert, F.; Arlt, W. COSMO-RS: An Alternative to Simulation for Calculating Thermodynamic Properties of Liquid Mixtures. *Annu. Rev. Chem. Biomol. Eng.* **2010**, *1*, 101−122.
(42) Klamt, A. The COSMO and COSMO-RS Solvation Models. *Wiley Interdiscip. Rev. Comput. Mol. Sci.* **2011**, *1*, 699−709.
(43) Klamt, A.; Schüürmann, G. COSMO: A New Approach to Dielectric Screening in Solvents with Explicit Expressions for the Screening Energy and its Gradient. *J. Chem. Soc., Perkin Trans.* **1993**, *2*, 799−805.
(44) Schäfer, A.; Klamt, A.; Sattel, D.; Lohrenz, J. C.; Eckert, F. COSMO Implementation in TURBOMOLE: Extension of an Efficient Quantum Chemical Code towards Liquid Systems. *Phys. Chem. Chem. Phys.* **2000**, *2*, 2187−2193.
(45) Klamt, A.; Eckert, F.; Diedenhofen, M.; Beck, M. E. First Principles Calculations of Aqueous pKa Values for Organic and Inorganic Acids Using COSMO-RS Reveal an Inconsistency in the Slope of the pKa Scale. *J. Phys. Chem. A* **2003**, *107*, 9380−9386.
(46) Eckert, F.; Klamt, A. Accurate Prediction of Basicity in Aqueous Solution with COSMO-RS. *J. Comput. Chem.* **2006**, *27*, 11−19.
(47) Eckert, F.; Leito, I.; Kaljurand, I.; Kütt, A.; Klamt, A.; Diedenhofen, M. Prediction of Acidity in Acetonitrile Solution with COSMO-RS. *J. Comput. Chem.* **2009**, *30*, 799−810.
(48) Sülzner, N.; Haberhauer, J.; Hättig, C.; Hellweg, A. Prediction of Acid pK_a Values in the Solvent Acetone based on COSMO-RS. *J. Comput. Chem.* **2022**, *43*, 1011−1022.
(49) Granucci, G.; Hynes, J. T.; Millié, P.; Tran-Thi, T.-H. A Theoretical Investigation of Excited-State Acidity of Phenol and Cyanophenols. *J. Am. Chem. Soc.* **2000**, *122*, 12243−12253.

https://doi.org/10.1021/acs.jpca.2c04436
J. Phys. Chem. A XXXX, XXX, XXX−XXX

(50) Agmon, N.; Rettig, W.; Groth, C. Electronic Determinants of Photoacidity in Cyanonaphthols. *J. Am. Chem. Soc.* **2002**, *124*, 1089−1096.
(51) Jacquemin, D.; Perpète, E. A.; Ciofini, I.; Adamo, C. Fast and Reliable Theoretical Determination of pK_a* for Photoacids. *J. Phys. Chem. A* **2008**, *112*, 794−796.
(52) Le Bahers, T.; Adamo, C.; Ciofini, I. Photophysical Properties of 8-Hydroxyquinoline-5-sulfonic Acid as a Function of the pH: A TD-DFT Investigation. *J. Phys. Chem. A* **2010**, *114*, 5932−5939.
(53) Baranov, M. S.; Lukyanov, K. A.; Borissova, A. O.; Shamir, J.; Kosenkov, D.; Slipchenko, L. V.; Tolbert, L. M.; Yampolsky, I. V.; Solntsev, K. M. Conformationally Locked Chromophores as Models of Excited-State Proton Transfer in Fluorescent Proteins. *J. Am. Chem. Soc.* **2012**, *134*, 6025−6032.
(54) Brémond, É.; Alberto, M. E.; Russo, N.; Ricci, G.; Ciofini, I.; Adamo, C. Photophysical Properties of NIR-emitting Fluorescence Probes: Insights from TD-DFT. *Phys. Chem. Chem. Phys.* **2013**, *15*, 10019−10027.
(55) Houari, Y.; Jacquemin, D.; Laurent, A. D. Methodological Keys for Accurate Simulations. *Phys. Chem. Chem. Phys.* **2013**, *15*, 11875−11882.
(56) Houari, Y.; Jacquemin, D.; Laurent, A. D. TD-DFT study of the pK_a* for Coumarins. *Chem. Phys. Lett.* **2013**, *583*, 218−221.
(57) Gao, J.; Li, N.; Freindorf, M. Hybrid QM/MM Simulations Yield the Ground and Excited State pK_a Difference: Phenol in Aqueous Solution. *J. Am. Chem. Soc.* **1996**, *118*, 4912−4913.
(58) Gao, J.; Byun, K. Solvent Effects on the $n\pi^*$ Transition of Pyrimidine in Aqueous Solution. *Theor. Chem. Acc.* **1997**, *96*, 151−156.
(59) Borg, O. A.; Durbeej, B. Relative Ground and Excited-State pK_a Values of Phytochromobilin in the Photoactivation of Phytochrome: A Computational Study. *J. Phys. Chem. B* **2007**, *111*, 11554−11565.
(60) Anders Borg, O.; Durbeej, B. Which Factors Determine the Acidity of the Phytochromobilin Chromophore of Plant Phytochrome? *Phys. Chem. Chem. Phys.* **2008**, *10*, 2528−2537.
(61) Tran-Thi, T.-H.; Prayer, C.; Millié, P.; Uznanski, P.; Hynes, J. T. Substituent and Solvent Effects on the Nature of the Transitions of Pyrenol and Pyranine. Identification of an Intermediate in the Excited-State Proton-Transfer Reaction. *J. Phys. Chem. A* **2002**, *106*, 2244−2255.
(62) Savarese, M.; Netti, P. A.; Adamo, C.; Rega, N.; Ciofini, I. Exploring the Metric of Excited State Proton Transfer Reactions. *J. Phys. Chem. B* **2013**, *117*, 16165−16173.
(63) Savarese, M.; Netti, P. A.; Rega, N.; Adamo, C.; Ciofini, I. Intermolecular Proton Shuttling in Excited State Proton Transfer Reactions: Insights from Theory. *Phys. Chem. Chem. Phys.* **2014**, *16*, 8661−8666.
(64) Laurent, A. D.; Houari, Y.; Carvalho, P. H. P. R.; Neto, B. A. D.; Jacquemin, D. ESIPT or not ESIPT? Revisiting Recent Results on 2,1,3-Benzothiadiazole under the TD-DFT Light. *RSC Adv.* **2014**, *4*, 14189−14192.
(65) Houari, Y.; Chibani, S.; Jacquemin, D.; Laurent, A. D. TD-DFT Assessment of the Excited State Intramolecular Proton Transfer in Hydroxyphenylbenzimidazole (HBI) Dyes. *J. Phys. Chem. B* **2015**, *119*, 2180−2192.
(66) Raucci, U.; Savarese, M.; Adamo, C.; Ciofini, I.; Rega, N. Intrinsic and Dynamical Reaction Pathways of an Excited State Proton Transfer. *J. Phys. Chem. B* **2015**, *119*, 2650−2657.
(67) Zhao, J.; Yao, H.; Liu, J.; Hoffmann, M. R. New Excited-State Proton Transfer Mechanisms for 1,8-Dihydroxydibenzo[a,h]-phenazine. *J. Phys. Chem. A* **2015**, *119*, 681−688.
(68) Cimino, P.; Raucci, U.; Donati, G.; Chiariello, M. G.; Schiazza, M.; Coppola, F.; Rega, N. On the Different Strength of Photoacids. *Theor. Chem. Acc.* **2016**, *135*, 1−12.
(69) Zhou, P.; Han, K. Unraveling the Detailed Mechanism of Excited-State Proton Transfer. *Acc. Chem. Res.* **2018**, *51*, 1681−1690.
(70) Chiariello, M. G.; Rega, N. Exploring Nuclear Photorelaxation of Pyranine in Aqueous Solution: an Integrated Ab-Initio Molecular Dynamics and Time Resolved Vibrational Analysis Approach. *J. Phys. Chem. A* **2018**, *122*, 2884−2893.
(71) Chiariello, M. G.; Donati, G.; Rega, N. Time-Resolved Vibrational Analysis of Excited State Ab Initio Molecular Dynamics to Understand Photorelaxation: The Case of the Pyranine Photoacid in Aqueous Solution. *J. Chem. Theory Comput.* **2020**, *16*, 6007−6013.
(72) Chiariello, M. G.; Raucci, U.; Donati, G.; Rega, N. Water-Mediated Excited State Proton Transfer of Pyranine−Acetate in Aqueous Solution: Vibrational Fingerprints from Ab Initio Molecular Dynamics. *J. Phys. Chem. A* **2021**, *125*, 3569−3578.
(73) Chiariello, M. G.; Donati, G.; Raucci, U.; Perrella, F.; Rega, N. Structural Origin and Vibrational Fingerprints of the Ultrafast Excited State Proton Transfer of the Pyranine-Acetate Complex in Aqueous Solution. *J. Phys. Chem. B* **2021**, *125*, 10273−10281.
(74) Thomaz, J. E.; Walker, A. R.; Van Wyck, S. J.; Meisner, J.; Martinez, T. J.; Fayer, M. D. Proton Transfer Dynamics in the Aprotic Proton Accepting Solvent 1-Methylimidazole. *J. Phys. Chem. B* **2020**, *124*, 7897−7908.
(75) Walker, A. R.; Wu, B.; Meisner, J.; Fayer, M. D.; Martínez, T. J. Proton Transfer from a Photoacid to a Water Wire: First Principles Simulations and Fast Fluorescence Spectroscopy. *J. Phys. Chem. B* **2021**, *125*, 12539−12551.
(76) Raucci, U.; Chiariello, M. G.; Rega, N. Modeling Excited-State Proton Transfer to Solvent: A Dynamics Study of a Super Photoacid with a Hybrid Implicit/Explicit Solvent Model. *J. Chem. Theory Comput.* **2020**, *16*, 7033−7043.
(77) Sobolewski, A. L.; Domcke, W.; Hättig, C. Photophysics of Organic Photostabilizers. Ab Initio Study of the Excited-State Deactivation Mechanisms of 2-(2'-Hydroxyphenyl)benzotriazole. *J. Phys. Chem. A* **2006**, *110*, 6301−6306.
(78) Acharya, A.; Chaudhuri, S.; Batista, V. S. Can TDDFT Describe Excited Electronic States of Naphthol Photoacids? A Closer Look with EOM-CCSD. *J. Chem. Theory Comput.* **2018**, *14*, 867−876.
(79) Grandjean, A.; Pérez Lustres, J. L.; Muth, S.; Maus, D.; Jung, G. Steady-State Spectroscopy to Single Out the Contact Ion Pair in Excited-State Proton Transfer. *J. Phys. Chem. Lett.* **2021**, *12*, 1683−1689.
(80) Grandjean, A.; Pérez Lustres, J. L.; Jung, G. Solvent-Controlled Intermolecular Proton-Transfer Follows an Irreversible Eigen-Weller Model from fs to ns. *ChemPhotoChem.* **2021**, *5*, 1094−1105.
(81) Sülzner, N.; Geissler, B.; Grandjean, A.; Jung, G.; Nuernberger, P. Excited-State Proton Transfer Dynamics of a Super-Photoacid in Acetone-Water Mixtures. *ChemPhotoChem.* **2022**, *6*, No. e202200041.
(82) Knorr, J.; Sülzner, N.; Geissler, B.; Spies, C.; Finkler, B.; Jung, G.; Nuernberger, P. Ultrafast transient absorption and solvation of a super-photoacid in acetoneous environments. *Photochem. Photobiol. Sci.* **2022**, DOI: 10.1007/s43630-022-00287-z.
(83) *TURBOMOLE*, V7.4 2019, a development of University of Karlsruhe and Forschungszentrum Karlsruhe GmbH, 1989−2007, TURBOMOLE GmbH, since 2007; available from http://www.turbomole.com.
(84) Balasubramani, S. G.; Chen, G. P.; Coriani, S.; Diedenhofen, M.; Frank, M. S.; Franzke, Y. J.; Furche, F.; Grotjahn, R.; Harding, M. E.; Hättig, C.; et al. TURBOMOLE: Modular Program Suite for Ab Initio Quantum-Chemical and Condensed-Matter Simulations. *J. Chem. Phys.* **2020**, *152*, 184107.
(85) Schwabe, T.; Sneskov, K.; Haugaard Olsen, J. M.; Kongsted, J.; Christiansen, O.; Hättig, C. PERI−CC2: A Polarizable Embedded RI-CC2Method. *J. Chem. Theory Comput.* **2012**, *8*, 3274−3283.
(86) Karbalaei Khani, S.; Marefat Khah, A.; Hättig, C. Comparison of Reaction Field Schemes for Coupling Continuum Solvation Models with Wave Function Methods for Excitation Energies. *J. Chem. Theory Comput.* **2020**, *16*, 4554−4564.
(87) Sülzner, N.; Hättig, C. Raw Data to "Theoretical Study on the Photoacidity of Hydroxypyrene Derivatives in DMSO Using ADC(2) and CC2". *Zenodo* 2022, DOI: 10.5281/zenodo.6598713.
(88) *BIOVIA COSMOconf*, Release 2021; Dassault Systèmes. http://www.3ds.com.
(89) *BIOVIA COSMOtherm*, Release 2021; Dassault Systèmes. http://www.3ds.com.

https://doi.org/10.1021/acs.jpca.2c04436
J. Phys. Chem. A XXXX, XXX, XXX−XXX

(90) Hellweg, A.; Eckert, F. Brick by Brick Computation of the Gibbs Free Energy of Reaction in Solution using Quantum Chemistry and COSMO-RS. *AIChE J.* **2017**, *63*, 3944−3954.
(91) Klamt, A.; Diedenhofen, M. A Refined Cavity Construction Algorithm for the Conductor-like Screening Model. *J. Comput. Chem.* **2018**, *39*, 1648−1655.
(92) Dunning, T. H. Gaussian Basis Sets for Tse in Correlated Molecular Calculations. I. The Atoms Boron through Neon and Hydrogen. *J. Chem. Phys.* **1989**, *90*, 1007−1023.
(93) Woon, D. E.; Dunning, T. H. Gaussian Basis Sets for Use in Correlated Molecular Calculations. III. The Atoms Aluminum through Argon. *J. Chem. Phys.* **1993**, *98*, 1358−1371.
(94) Weigend, F.; Häser, M. RI-MP2: First Derivatives and Global Consistency. *Theor. Chem. Acc.* **1997**, *97*, 331−340.
(95) Hättig, C.; Hellweg, A.; Köhn, A. Distributed Memory Parallel Implementation of Energies and Gradients for Second-Order Møller-Plesset Perturbation Theory with the Resolution-of-the-Identity Approximation. *Phys. Chem. Chem. Phys.* **2006**, *8*, 1159−1169.
(96) Hättig, C. Geometry Optimizations with the Coupled-Cluster Model CC2 using the Resolution-of-the-Identity Approximation. *J. Chem. Phys.* **2003**, *118*, 7751−7761.
(97) Cammi, R.; Mennucci, B.; Tomasi, J. Second-Order Møller-Plesset Analytical Derivatives for the Polarizable Continuum Model Using the Relaxed Density Approach. *J. Phys. Chem. A* **1999**, *103*, 9100−9108.
(98) Karbalaei Khani, S.; Marefat Khah, A.; Hättig, C. COSMO-RI-ADC(2) Excitation Energies and Excited State Gradients. *Phys. Chem. Chem. Phys.* **2018**, *20*, 16354−16363.
(99) Köhn, A.; Hättig, C. Analytic Gradients for Excited States in the Coupled-Cluster Model CC2 Employing the Resolution-of-the-Identity Approximation. *J. Chem. Phys.* **2003**, *119*, 5021−5036.
(100) Kendall, R. A.; Dunning, T. H.; Harrison, R. J. Electron Affinities of the First-Row Atoms Revisited. Systematic Basis Sets and Wave Functions. *J. Chem. Phys.* **1992**, *96*, 6796−6806.
(101) Hättig, C. In Response Theory and Molecular Properties (A Tribute to Jan Linderberg and Poul Jørgensen). *Adv. Quantum Chem.* **2005**, *50*, 37−60.
(102) Hättig, C.; Weigend, F. CC2 Excitation Energy Calculations on Large Molecules using the Resolution of the Identity Approximation. *J. Chem. Phys.* **2000**, *113*, 5154−5161.
(103) Jacquemin, D. What is the Key for Accurate Absorption and Emission Calculations, Energy or Geometry? *J. Chem. Theory Comput.* **2018**, *14*, 1534−1543.
(104) Wen, Z.; Karas, L. J.; Wu, C.-H.; Wu, J. I.-C. How does Excited-State Antiaromaticity Affect the Acidity Strengths of Photoacids? *Chem. Commun.* **2020**, *56*, 8380−8383.
(105) Haynes, W. M.; Lide, D. R.; Bruno, T. J. *CRC Handbook of Chemistry and Physics*, 97th ed.; CRC Press: Boca Raton, FL, 2016.
(106) Schreiber, M.; Silva-Junior, M. R.; Sauer, S. P. A.; Thiel, W. Benchmarks for Electronically Excited States: CASPT2, CC2, CCSD, and CC3. *J. Chem. Phys.* **2008**, *128*, 134110.
(107) Winter, N. O. C.; Graf, N. K.; Leutwyler, S.; Hättig, C. Benchmarks for 0−0 Transitions of Aromatic Organic Molecules: DFT/B3LYP, ADC(2), CC2, SOS-CC2 and SCS-CC2 Compared to High-Resolution Gas-Phase Data. *Phys. Chem. Chem. Phys.* **2013**, *15*, 6623−6630.

https://doi.org/10.1021/acs.jpca.2c04436
J. Phys. Chem. A XXXX, XXX, XXX−XXX